XV International Conference on Computational Plasticity. Fundamentals and Applications
COMPLAS 2019
E. Oñate, D.R.J. Owen, D. Peric, M. Chiumenti & Eduardo de Souza Neto (Eds)

A FINITE STRAIN THERMO-MECHANICALLY COUPLED MATERIAL MODEL FOR SEMI-CRYSTALLINE POLYMERS

SEBASTIAN FELDER*, HAGEN HOLTHUSEN*, STEFAN HESSELER†, FELIX POHLKEMPER†, JAAN-WILLEM SIMON*, THOMAS GRIES† AND STEFANIE REESE*

* Institute of Applied Mechanics (IFAM)
RWTH Aachen University
Mies-van-der-Rohe-Str. 1, 52074 Aachen, Germany
e-mail: sebastian.felder@rwth-aachen.de, web page: https://www.ifam.rwth-aachen.de/

† Institut für Textiltechnik (ITA)
RWTH Aachen University
Otto-Blumenthal-Str. 1, 52074 Aachen, Germany
web page: https://www.ita.rwth-aachen.de

Key words: Semi-crystalline polymers, Thermo-mechanical coupling, Finite strains, Crystallisation kinetics

Abstract. In this work, a thermo-mechanically coupled constitutive model for semi-crystalline polymers is derived in a thermodynamically consistent manner. In general, the macroscopic material behaviour of this class of materials is dictated by the underlying microstructure, i.e. by the distribution and structure of crystalline regimes, which form up after cooling from the amorphous melt. In order to account for the latter, the total degree of crystallinity is incorporated as an internal variable and its evolution is prescribed by means of a non-isothermal crystallisation kinetics model. The numerically efficient and robust framework is characterised based on experimental data for Polyamide 6 and shows a promising potential to predict the hyperelastic, visco-plastic material behaviour at various temperatures.

1 INTRODUCTION

Thermoplastic polymers are an important class of materials for many technically relevant applications. In contrast to thermosets, which form irreversible chemical bonds, they can be repeatedly reshaped after heating above the melting point. As a consequence, they are well-suited for forming processes. A specific class of thermoplastics are semi-crystalline polymers (e.g. Polyamide 6, which is the considered polymer in this work), which partly crystallise after cooling from the melt. The degree and structure of the crystalline regimes depends on the thermal conditions and applied stress. The relative degree of crystallinity χ_c can be determined by the heat flow rate $(dh)/(dt)$, which is measured by differential

scanning calorimetry (DSC) (cf. chapter 3) and lays between zero (100% amorphous, $t < t_{On}$) and one (at the end of the crystallisation process, $t > t_{End}$).

$$\chi_c = \frac{\int_{t_{\mathrm{On}}}^{t} \frac{dh}{dt} dt}{\int_{t_{\mathrm{On}}}^{t_{\mathrm{End}}} \frac{dh}{dt} dt} := \frac{\Delta h_t}{\Delta h_m}, \quad \chi = \frac{\int_{t_{\mathrm{On}}}^{t} \frac{dh}{dt} dt}{\Delta h_f^{100}} = \chi_c \, \frac{\Delta h_m}{\Delta h_f^{100}} \tag{1}$$

Here, the change in enthalpy during the whole crystallisation process $\Delta h_m(\dot{\theta})$ is introduced, which is depending on the cooling rate. To obtain the absolute degree of crystallinity χ, the material constant Δh_f^{100} corresponding to the specific fusion enthalpy of a 100% crystalline material, must be determined. For Polyamide 6 the latter can be computed from the average of the values corresponding to the α-form (241 J/g) and γ-form (239 J/g) as suggested by Fornes et al. [1].
Naturally, the morphology of the underlying microstructure (i.e. the degree of crystallinity) has a significant influence on the mechanical behaviour of semi-crystalline polymers (cf. chapter 3). Furthermore, the mechanical response of Polyamide 6 is characterised by non-linear, visco-plastic behaviour, depending on the thermal conditions and accompanied by large elastic and plastic strains (cf. section 3). In order to avoid cost- and time-consuming trial and error approaches, a strong demand for computational models arises, which accurately predict the complex material and structural response of parts during and after thermoforming processes.
To this end, a continuum-mechanical, phenomenological material model is presented in this work. The thermo-mechanically coupled, visco-plastic constitutive framework is derived in a thermodynamically consistent manner (cf. chapter 2) and valid for large deformation. In order to account for the underlying microstructure, the total degree of crystallinity χ is treated as an additional internal variable. Crystallisation from a relaxed, static melt is assumed and the evolution of χ is modelled by means of a non-isothermal representation of the Avrami equation (see section 2.1). In section 3, the model is characterised by isothermal and non-isothermal DSC analysis and uniaxial tensile tests for different loading rates and degrees of crystallinity at varying temperatures .

2 MATERIAL MODEL FORMULATION

In line with e.g. the work [2] the resistance of deformation is decomposed into an intermolecular and a network contribution. For the intermolecular resistance, a finite strain elasto-plastic model with non-linear isotropic hardening and non-linear kinematic hardening of Frederick Armstrong type is considered. To account for the molecular orientation and relaxation, the molecular network resistance is represented by a finite strain visco-elastic model. Quantities corresponding to the elasto-plastic model and to the viscous model will be denoted with index $\mathtt{1}$ and $\mathtt{2}$, respectively.
The total deformation gradient $\boldsymbol{F}$ is multiplicatively decomposed separately for both models. For the elasto-plastic constitutive framework the classical split of the deformation gradient, $\boldsymbol{F} = \boldsymbol{F}_{e\mathtt{1}} \boldsymbol{F}_p$, into its elastic part $\boldsymbol{F}_{e\mathtt{1}}$ and plastic part $\boldsymbol{F}_p$ is proposed To account for non-linear kinematic hardening, a physically motivated additional split of the plastic part $\boldsymbol{F_p} = \boldsymbol{F}_{pe} \boldsymbol{F}_{pi}$ is performed. Noteworthy, these decompositions result in

the intermediate plastic configuration ic_{1a} and the so-called intermediate configuration of kinematic hardening ic_{1b}. The kinematic relations corresponding to the viscous model are based on a multiplicative decomposition of the deformation gradient, $\boldsymbol{F} = \boldsymbol{F}_{e2}\boldsymbol{F}_i$, into its elastic $\boldsymbol{F}_{e2}$ and inelastic part $\boldsymbol{F}_i$. Thus, an additional, inelastic intermediate configuration ic_2 is introduced.
The Helmholtz free energy depends on the deformation only through the elastic right Cauchy-Green deformation tensors $\boldsymbol{C}_{e1}$, $\boldsymbol{C}_{e2}$, and $\boldsymbol{C}_{pe}$, in agreement with the principal of material frame invariance.

$$\boldsymbol{C}_{e1} = \boldsymbol{F}_{e1}^T\boldsymbol{F}_{e1} = \boldsymbol{F}_p^{-T}\boldsymbol{C}\boldsymbol{F}_p^{-1}, \quad \boldsymbol{C}_{e2} = \boldsymbol{F}_{e2}^T\boldsymbol{F}_{e2} = \boldsymbol{F}_i^{-T}\boldsymbol{C}\boldsymbol{F}_i^{-1}, \quad \boldsymbol{C}_{pe} = \boldsymbol{F}_{pe}^T\boldsymbol{F}_{pe} = \boldsymbol{F}_{pi}^{-T}\boldsymbol{C}_p\boldsymbol{F}_{pi}^{-1} \tag{2}$$

Here the right Cauchy-Green tensor $\boldsymbol{C} = \boldsymbol{F}^T\boldsymbol{F}$ and the plastic right Cauchy-Green tensor $\boldsymbol{C}_p = \boldsymbol{F}_p^T\boldsymbol{F}_p$ are introduced. The total, specific Helmholtz free energy is additively decomposed into a contribution stemming from the intermolecular resistance ψ_1, a contribution from the molecular network resistance ψ_2 and an energy term ψ_χ associated with the crystallisation process.

$$\psi = \underbrace{\psi_{e1}(\boldsymbol{C}_{e1}, \chi, \theta) + \psi_{kin}(\boldsymbol{C}_{pe}, \theta) + \psi_{iso}(\kappa, \chi, \theta)}_{\psi_1} + \psi_2(\boldsymbol{C}_{e2}, \chi, \theta) + \psi_\chi(\chi, \theta) \tag{3}$$

To account for the dependence of the material response on the temperature θ and the morphology of the underlying microstructure, the energy terms are functions of the temperature θ and the total degree of crystallinity χ. In this work, no differentiation between crystal configurations nor morphology (lamella thickness) is made. Furthermore, non-isothermal crystallisation processes from a static, relaxed melt are assumed. Consequently, $\chi(\theta, \dot{\theta})$ is introduced as an additional internal variable and assumed to be a function of the temperature and cooling rate $\dot{\theta}$. Hence, the free energy is an implicit function of the cooling rate. In equation (3), ψ_{e1} and ψ_{e2} denote the elastic energy contributions of the intermolecular and molecular network resistances, respectively. To phenomenologically account for Bauschinger-like phenomena, ψ_{kin}, a defect-energy associated with plastic deformations, is introduced. The stored energy due to isotropic hardening is defined as ψ_{iso} and is a function of the accumulated plastic strain κ.

2.1 Derivation based on the Clausius-Duhem inequality

Starting point of the thermodynamic consistent derivation of the constitutive framework is the Clausius-Duhem form of the entropy inequality with respect to the reference configuration (rc).

$$\boldsymbol{S} : \frac{1}{2}\dot{\boldsymbol{C}} - \rho_0(\dot{\psi} + \eta_S\dot{\theta}) - \frac{1}{\theta}\boldsymbol{q}_0 \cdot \mathrm{Grad}(\theta) \geq 0 \tag{4}$$

Here, $\boldsymbol{S}$ denotes the second Piola-Kirchhoff stress, η_S is the specific entropy, ρ_0 is the density in the rc and $\boldsymbol{q}_0$ the heat flux with respect to the rc. Assuming that ψ_{e1}, ψ_{e2} and ψ_{kin} are isotropic functions of $\boldsymbol{C}_{e1}$, $\boldsymbol{C}_{e2}$, and $\boldsymbol{C}_{pe}$, respectively, and inserting the total time derivative of the Helmholtz free energy (3) into the latter expression yields, after several

mathematical transformations, the following form of the Clausius-Duhem inequality.

$$\begin{aligned}&(\boldsymbol{S}-\boldsymbol{S}_1-\boldsymbol{S}_2):\frac{1}{2}\dot{\boldsymbol{C}}-\rho_0\left(\frac{\partial\psi}{\partial\theta}+\eta_S\right)\dot{\theta}-\frac{1}{\theta}\boldsymbol{q}_0\cdot\mathrm{Grad}(\theta)\\&-\rho_0\frac{\partial\psi}{\partial\chi}\dot{\chi}+\boldsymbol{M}_2:\boldsymbol{D}_i+\left(\boldsymbol{M}_1-\bar{\boldsymbol{X}}\right):\boldsymbol{D}_p+\boldsymbol{M}_{kin}:\boldsymbol{D}_{pi}+R\dot{\kappa}\geq 0\end{aligned}\tag{5}$$

The inequality (5) is an expression of the evolution of the internal variables (i.e. $\dot{\chi}$, $\boldsymbol{D}_i$, $\boldsymbol{D}_p$, $\boldsymbol{D}_{pi}$, and $\dot{\kappa}$) and the thermodynamic conjugated forces. Here, $\boldsymbol{D}_{(*)}=\mathrm{sym}(\boldsymbol{L}_{(*)})$ denotes the symmetric part of the corresponding velocity gradient $\boldsymbol{L}_{(*)}=\dot{\boldsymbol{F}}_{(*)}\boldsymbol{F}_{(*)}^{-1}$, with $(*)=i,p,pi$. The second Piola-Kirchhoff stress tensors corresponding to the intermolecular and molecular network resistance are

$$\boldsymbol{S}_1=2\rho_0\boldsymbol{F}_p^{-1}\frac{\partial\psi_{e1}}{\partial\boldsymbol{C}_{e1}}\boldsymbol{F}_p^{-T},\quad \boldsymbol{S}_2=2\rho_0\boldsymbol{F}_i^{-1}\frac{\partial\psi_2}{\partial\boldsymbol{C}_{e2}}\boldsymbol{F}_i^{-T}\tag{6}$$

respectively. The Mandel stress tensors

$$\boldsymbol{M}_1=2\rho_0\boldsymbol{C}_{e1}\frac{\partial\psi_{e1}}{\partial\boldsymbol{C}_{e1}},\quad \boldsymbol{M}_2=2\rho_0\boldsymbol{C}_{e2}\frac{\partial\psi_2}{\partial\boldsymbol{C}_{e2}}\tag{7}$$

are defined with respect to the intermediate states ic_1 and ic_2, respectively. In addition, the back stress $\bar{\boldsymbol{X}}$ in ic_{1a}, the Mandel stress corresponding to kinematic hardening $\boldsymbol{M}_{kin}$ in ic_{1b}, and the stress-like driving force of isotropic hardening R read

$$\bar{\boldsymbol{X}}=2\rho_0\boldsymbol{F}_{pe}\frac{\partial\psi_{kin}}{\partial\boldsymbol{C}_{pe}}\boldsymbol{F}_{pe}^T,\quad \boldsymbol{M}_{kin}=2\rho_0\boldsymbol{C}_{pe}\frac{\partial\psi_{kin}}{\partial\boldsymbol{C}_{pe}},\quad R=-\rho_0\frac{\partial\psi_{iso}}{\partial\kappa}\tag{8}$$

In order to fulfil the first line of the inequality (5) for arbitrary processes, the following relations for the total second Piola-Kirchhoff stress and entropy must hold

$$\boldsymbol{S}=\boldsymbol{S}_1+\boldsymbol{S}_2,\qquad \eta_S=-\frac{\partial\psi}{\partial\theta}\tag{9}$$

Fourier's law , $\boldsymbol{q}_0=-J\lambda_T\boldsymbol{C}^{-1}\mathrm{Grad}(\theta)$, is applied in addition for the heat flux, referring to the rc, where λ_T denotes the heat conductivity and $J=\det\boldsymbol{F}$ holds.
To guarantee the non-negativeness of internal dissipation (the second line in inequality (5)), a set of evolution equations for the internal variables is presented, which fulfils the inequality. Based on the proposed formulation of Reese and Govindjee [3], the evolution of the inelastic deformation is given by

$$\boldsymbol{D}_i=\frac{1}{2\tau\mu_2}\left(\boldsymbol{M}_2-\frac{1}{3}\mathrm{tr}(\boldsymbol{M}_2)\boldsymbol{I}\right)+\frac{1}{9\tau K_2}\mathrm{tr}(\boldsymbol{M}_2)\boldsymbol{I}.\tag{10}$$

In the latter expression, the bulk modulus and shear modulus corresponding to the molecular network resistance are denoted by $K_2(\theta)$ and $\mu_2(\theta)$, respectively. The relaxation time $\tau(\boldsymbol{S}_2,\boldsymbol{C},\theta,\chi)$ must be greater than zero and is in general a non-linear function of $\boldsymbol{S}_2$, $\boldsymbol{C}$,

θ, and χ.
In this work no pressure dependence, nor tension-compression asymmetry of the yield behaviour is assumed. Hence, a yield function of von Mises type is proposed

$$\Phi = ||\mathrm{dev}(\boldsymbol{M}_1) - \mathrm{dev}(\bar{\boldsymbol{X}})|| - \sqrt{\frac{2}{3}}(\sigma_y - R) \tag{11}$$

Here, the initial yield stress $\sigma_y(\theta, \chi)$ is introduced and dev$(*)$ denotes the deviatoric part of a quantity. The associative plastic flow rule and the evolution equations for kinematic and isotropic hardening are

$$\boldsymbol{D}_p = \dot{\lambda}\frac{\partial \Phi}{\partial \boldsymbol{M}_1} = \dot{\lambda}\frac{\mathrm{dev}(\boldsymbol{M}_1) - \mathrm{dev}(\bar{\boldsymbol{X}})}{||\mathrm{dev}(\boldsymbol{M}_1) - \mathrm{dev}(\bar{\boldsymbol{X}})||}, \quad \boldsymbol{D}_{pi} = \dot{\lambda}\frac{b}{c}\mathrm{dev}(\boldsymbol{M}_{kin}), \quad \dot{\kappa} = \dot{\lambda}\frac{\partial \Phi}{\partial R} = \sqrt{\frac{2}{3}}\dot{\lambda} \tag{12}$$

respectively, where $\dot{\lambda}$ is the plastic multiplier. The equation for $\boldsymbol{D}_{pi}$ represents nonlinear kinematic hardening of Armstrong-Frederick type in which $b(\theta)$ and $c(\theta)$ are material parameters. Finally, the elasto-plastic model is supplemented by the Kuhn-Tucker conditions $\Phi \leq 0$, $\dot{\lambda} \geq 0$, and $\Phi\dot{\lambda} = 0$.
To predict the relative degree of crystallinity χ_c, the non-isothermal representation of the Avrami equation by means of the modified Nakamura-Ziabicki framework [4] was found to be a well-suited model (cf. chapter 3). Inserting the proposed form into the relation for the total degree of crystallinity χ (cf. equation 1) and differentiating the latter with respect to time yields the evolution equation for χ.

$$\dot{\chi} \approx \dot{\chi}_c\frac{\Delta h_m}{\Delta h_f^{100}} = n\ K_c(1-\chi_c)\left(\int_{t_{on}}^{t} K_c dt\right)^{n-1}\frac{\Delta h_m}{\Delta h_f^{100}} \geq 0 \tag{13}$$

The Avrami exponent n represents the nucleation mechanism and growth dimension and is assumed to be temperature independent. The temperature and cooling rate dependent parameter K_c is given by an empirical function proposed by [5]

$$K_c = K_{max}\ \exp\left(-\frac{4\ln(2)(\theta - \theta_{max})^2}{D^2}\right) \tag{14}$$

where the Nakamura-Ziabicki crystallisation parameters $K_{max}(\dot{\theta})$, $\theta_{max}(\dot{\theta})$ and $D(\dot{\theta})$ are depending on the cooling rate. The starting time of the crystallisation process t_{on} is determined by the cooling rate depending onset temperature $\theta_{on}(\dot{\theta})$.
It can be shown, that the set of evolution equations (10) and (12) fulfils the non-negativeness requirement of the Clausius-Duhem inequality (5) (cf. [3] and [6]). The thermodynamic consistency of the chosen evolution law for $\dot{\chi}$, will be discussed briefly. Concomitant with the assumption of a crystallisation process from a relaxed, static melt, the energy terms depending on the deformation (i.e. ψ_{e1}, ψ_{kin}, ψ_{iso}, and ψ_2) are zero if $\dot{\chi} > 0$. In addition, for the energy associated with transformation $\partial\psi_\chi/\partial\chi < 0$ holds if $\theta < \theta_{On}$ (cf. equation (20)) and thus the remaining inequality $-\rho_0(\partial\psi_\chi/\partial\chi)\dot{\chi} \geq 0$ is always fulfilled.

2.2 Specific choices for energy terms

To conclude the constitutive framework, a set of volumetric energy terms Ψ is specified in this section. For the elastic energy contribution of the molecular network resistance a compressible version of the widely used Arruda-Boyce model [7] is chosen

$$\Psi_2(\boldsymbol{C}_{e2},\theta) = K_2\left(\frac{J_{e2}^2-1}{4} - \ln(J_{e2})\left(\frac{1}{2}+3\alpha_{T2}(\theta-\theta_0)\right)\right) + \mu^*\sum_{i=1}^{5}\frac{C_i}{\lambda_m^{2i-2}}\left(\mathrm{tr}(\bar{\boldsymbol{C}}_{e2})^i - 3^i\right) \tag{15}$$

The latter expression is a function of the isochoric part $\bar{\boldsymbol{C}}_{e2} = \bar{\boldsymbol{F}}_{e2}^T\bar{\boldsymbol{F}}_{e2}$ of the elastic right Cauchy-Green tensor, where $\bar{\boldsymbol{F}}_{e2} = J_{e2}^{-\frac{1}{3}}\boldsymbol{F}_{e2}$ and $J_{e2} = \det\boldsymbol{F}_{e2} = \sqrt{\det\boldsymbol{C}_{e2}}$ holds. The constant parameter λ_m relates to the locking stretch of a fully extended chain, $\alpha_{T2}(\theta,\chi)$ is the coefficient of thermal expansion corresponding to the network resistance and θ_0 is a reference temperature. The parameter μ^* and the tuple C_i are defined as

$$\mu^* = \mu_2\frac{1}{1+\frac{3}{5\lambda_m^2}+\frac{99}{175\lambda_m^4}+\frac{513}{875\lambda_m^6}+\frac{42039}{67375\lambda_m^8}}, \quad C_i = \left(\tfrac{1}{2} \quad \tfrac{1}{20} \quad \tfrac{11}{1050} \quad \tfrac{19}{7000} \quad \tfrac{519}{67375}\right) \tag{16}$$

For the intermolecular resistance a Neo-Hookean material with combined linear and non-linear isotropic hardening of Voce type and non-linear kinematic hardening of Armstrong-Frederick type is considered. The corresponding energy terms are

$$\begin{aligned}\Psi_{e1} =& \frac{\mu_1}{2}\left(\mathrm{tr}(\boldsymbol{C}_{e1})-3\right) - \mu_1\ln(J_{e1}) + \frac{\Lambda_1}{4}\left(\det(\boldsymbol{C}_{e1}) - 1 - 2\ln(J_{e1})\right)\\ &- 3K_1\alpha_{T1}(\theta-\theta_0)\ln(J_{e1})\end{aligned} \tag{17}$$

$$\Psi_{kin} = \frac{c}{2}(\mathrm{tr}(\boldsymbol{C}_{pe})-3) - c\ln(J_{pe}) \tag{18}$$

$$\Psi_{iso} = (\sigma_\infty-\sigma_y)\left(\kappa+\frac{\exp(-\beta\kappa)}{\beta}\right) + \frac{1}{2}H\kappa^2 \tag{19}$$

where $J_{e1} = \det\boldsymbol{F}_{e1}$ is defined. The material parameters $\mu_1(\theta,\chi)$, $\Lambda_1(\theta,\chi)$, $K_1(\theta,\chi)$, $\alpha_{T1}(\theta,\chi)$, $\sigma_\infty(\theta,\chi)$, $\beta(\theta,\chi)$, and $H(\theta,\chi)$ corresponding to the elasto-plastic model, are the Lamé constants, bulk modulus, coefficient of thermal expansion, and isotropic hardening parameters, respectively. It is of note, that the specific functions for the introduced material parameters are provided in chapter 3. The specific energy associated with crystallisation, which contributes in an important manner to the heat release of fusion (cf. equation (21)), is given by

$$\psi_\chi = \Delta h_f^{100}\frac{\theta-\theta_{On}}{\theta_{On}}\chi \tag{20}$$

2.3 Heat generation due to dissipation and crystallisation

The heat generation r_t due to plastic r_1 and viscous dissipation r_2 and due to exothermic crystallisation r_χ is briefly discussed in this paragraph. The terms can be derived in a

consistent manner from the local form of the energy balance and the Helmholtz free energy

$$r_t = \underbrace{\left(\boldsymbol{M}_1 - \theta\frac{\partial \boldsymbol{M}_1}{\partial\theta} - \bar{\boldsymbol{X}} + \theta\frac{\partial \bar{\boldsymbol{X}}}{\partial\theta}\right) : \boldsymbol{D}_p + \left(\boldsymbol{M}_{kin} - \theta\frac{\partial \boldsymbol{M}_{kin}}{\partial\theta}\right) : \boldsymbol{D}_{pi} + \left(R - \theta\frac{\partial R}{\partial\theta}\right)\dot{\kappa}}_{r_1}$$
$$+ \underbrace{\left(\boldsymbol{M}_2 - \theta\frac{\partial \boldsymbol{M}_2}{\partial\theta}\right) : \boldsymbol{D}_i}_{r_2} + \underbrace{\rho_0\ \Delta h_f^{100}\ \dot{\chi}}_{r_\chi} \tag{21}$$

Noteworthy, the dissipation due to thermo-elastic coupling $(\partial \boldsymbol{S}/\partial\theta) : (1/2\dot{\boldsymbol{C}})$ is assumed to be negligibly small and is thus omitted in the latter expression.

2.4 Aspects of numerical implementation

For convenience the derivation of the constitutive equations was carried out in the intermediate configurations. However, for the numerical implementation as an user material subroutine *UMAT* into the commercial FEM software *ABAQUS*/Standard, the model equations need to be represented in the current configuration. To this end, several tensorial pull-back and push-forward operations are applied. The algorithmic implementation is based on the works of Dettmer and Reese [8] and Vladimirov et al. [6]. For the numerical integration of the evolution equations (10) and (12) the exponential map algorithm, which preserves plastic volume and the symmetry of the internal variables, is applied and a local system of 16 non-linear scalar equations is solved in an efficient manner. The evolution equation of the total degree of crystallinity is discretized by means of the implicit Euler method and the trapezoidal scheme is used to numerically approximate the integral in equation (13).

3 PARAMETER CALIBRATION

In this section, the characterisation procedure to obtain the material parameter set is discussed briefly. During the computational solution procedure, cubic spline interpolation is applied to interpolate between the parameters presented in the following.
In order to investigate the crystallisation kinetics of Polyamide 6 (*Ultramid B40*, kindly provided by BASF), isothermal (crystallisation at 192°C, 194°C, 196°C and 198°C) and non-isothermal DSC analysis (constant cooling rates of 5°C/min, 10°C/min, 20°C/min, 40°C/min, 60°C/min, and 100°C/min) are conducted with the *DSC 1* from *Mettler Toledo*. Based on the DSC data, the relative degree of crystallinty χ_c over time is computed (cf. equation 1). The constant Avrami exponent n =2.38 is obtained from linear regression of the classical double logarithmic form of the isothermal and non-isothermal DSC data. The remaining, cooling rate dependent parameters of the non-isothermal model (cf. equations (13) and (14)) are obtained from non-linear optimization of the non-isothermal DSC data and are depicted in table 1. The non-isothermal experimental data and the corresponding fit of the proposed model is shown in figure 1.

The mechanical parameters are obtained from uniaxial tensile test. Different loading

Table 1: Parameters for modified Nakamura-Ziabicki model determined by non-linear optimization

$\dot{\theta}$ [K/min]	K_{max} [1/min]	θ_{max} [K]	D [K]	Δh_m [J/g]
5	9.51	348.22	102.27	56.89
10	13.73	348.46	100.48	54.57
20	9.28	351.10	109.52	54.16
40	7.77	355.17	116.97	50.48
60	5.54	362.99	128.31	48.24
100	4.80	359.49	125.64	43.92

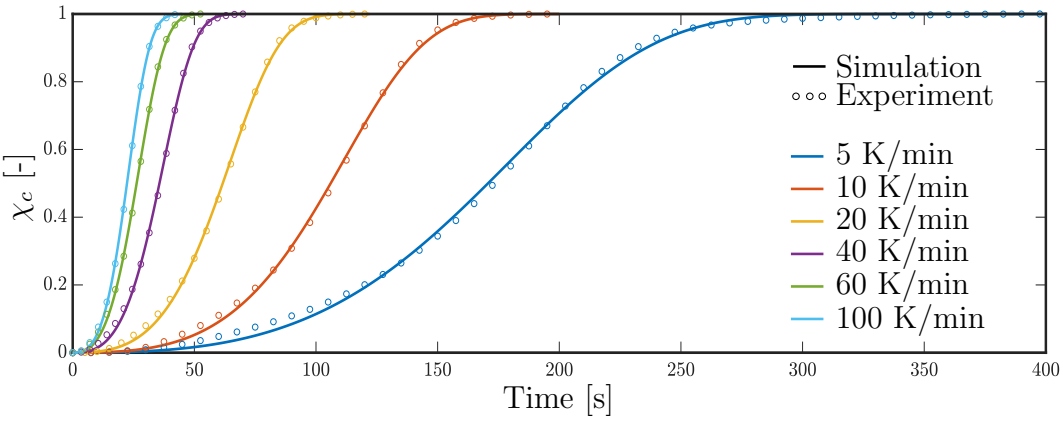

Figure 1: Non-isothermal DSC data and corresponding model response

procedures (monotonic loading, cyclic loading, and relaxation tests) at different loading rates ($v_{min} = 1$ mm/min and $v_{max} = 10$ mm/min) are performed at varying temperatures below and above the glass transition temperature ($\theta_g \approx 80$°C) at 20°C, 50°C, 120°C, and 160°C. Dried specimens (type 5A in accordance with ISO 527-2:2012), which have been produced by injection moulding, are tested for two different degrees of crystallinity (χ_{min}= 23 % and χ_{max}= 28 %). Digital image correlation (DIC) is applied to obtain the true stress (Cauchy stress σ_1) over stretch λ_1 relation in longitudinal 1-direction (cf. figure 2). Based on these results a staggered characterisation scheme is developed, in order to obtain a unique set of mechanical parameters for each considered temperature (cf. table 2). It should be noted that due to the lack of compression data no information about the Bauschinger effect is available. Consequently, only isotropic hardening is considered and the parameters corresponding to kinematic hardening i.e. c and b are set to very small values. Infrared thermography (IR) revealed a significant temperature increase, related to adiabatic self-heating, accompanied by thermal softening, for higher loading rates at moderate stretch levels of 5 %. Due to this fact, the (isothermal) material parameters are only fitted up to this point for v_{max}.

The experimental data for monotonic tensile test at different loading rates and for varying temperatures and degrees of crystallinity is depicted in figure 2, together with the

Table 2: Set of mechanical parameters at different temperatures

Function	Parameter at:	20 °C	50 °C	120 °C	160 °C
$E_1 = \chi E_{1,0}(\theta)$	$E_{1,0}$ [MPa]	5510	3923	1040	851
$E_2 = E_2(\theta)$	E_2 [MPa]	1210	703	130	75
$\nu_1 = \nu_2$	ν_1 [-]	0.35	0.35	0.35	0.35
$\sigma_y = \chi\sigma_{y,0}(\theta)$	$\sigma_{y,0}$ [MPa]	120	45	24	22
$\beta = \chi\beta_0(\theta)$	β_0 [-]	2712	2021	200	195
$H = \chi H_0(\theta)$	H_0 [MPa]	239	669	181	171
$\sigma_\infty = \chi^{\alpha(\theta)}\sigma_{\infty,0}(\theta)$	$\sigma_{\infty,0}$ [MPa]	57.5	66.0	715.0	716.0
	α [-]	0.154	0.682	2.651	2.425
$\tau = \tau_0(\theta)\|\boldsymbol{B}\|^{\varphi(\theta)}\exp(\|\boldsymbol{\sigma}_2\|)^{-\delta(\theta)}$	τ_0 [s]	463	220	96	72
	φ [-]	6.624	5.014	2.525	2.425
	δ [-]	0.196	0.277	0.421	0.621

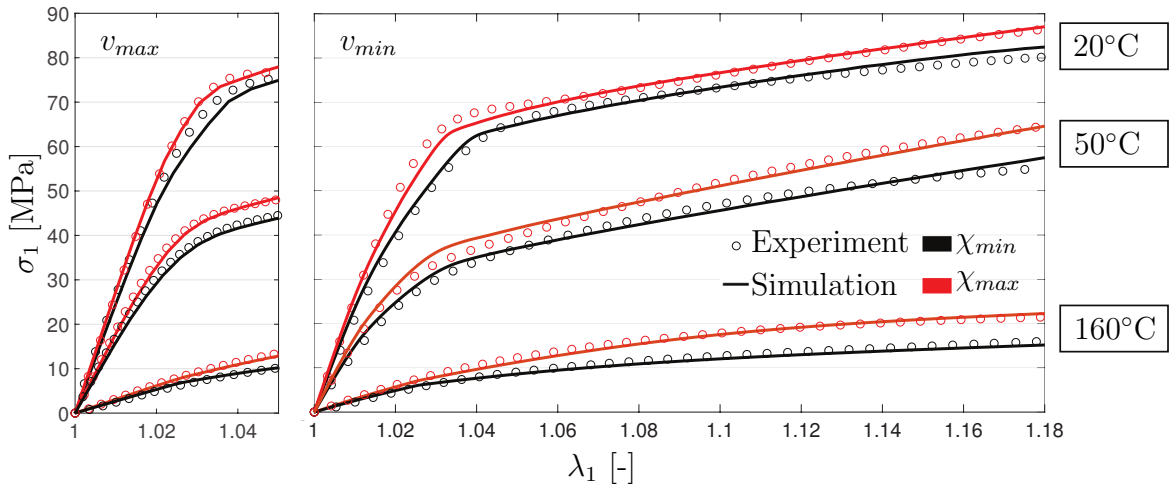

Figure 2: Monotonic, uniaxial extension - Experimental data and corresponding model response

corresponding fit of the proposed model.

The thermal material properties are obtained from the literature. Based on experimental investigations a constant heat conductivity is considered $\lambda_T = 0.27$ W/Km [9]. In line with the data provided in [1], the following function for the density is assumed $\rho_0 = \chi\, 0.001195 + (1-\chi)0.00109$ g/mm^3. For simplicity, the coefficient of thermal expansion is assumed to be constant $\alpha_1 = \alpha_2$=0.876·10^{-4} (cf. [10]). In line with the work [11], the following relation for the heat capacity is assumed $c_p = 4.502\theta + 138.7$ mJ/gK.

4 COMPUTATIONAL EXAMPLE

In order to investigate the crystallisation process and structural response, a thermo-mechanically coupled boundary value problem is considered. In two separate computations, the surface of a plate is subjected to different cooling rates (80 K/min and 15 K/min) until a temperature of 120 °C is reached at t_h (cf. figure 3). Next, the temperature is held constant for 50 s to obtain a homogeneous temperature field. Subse-

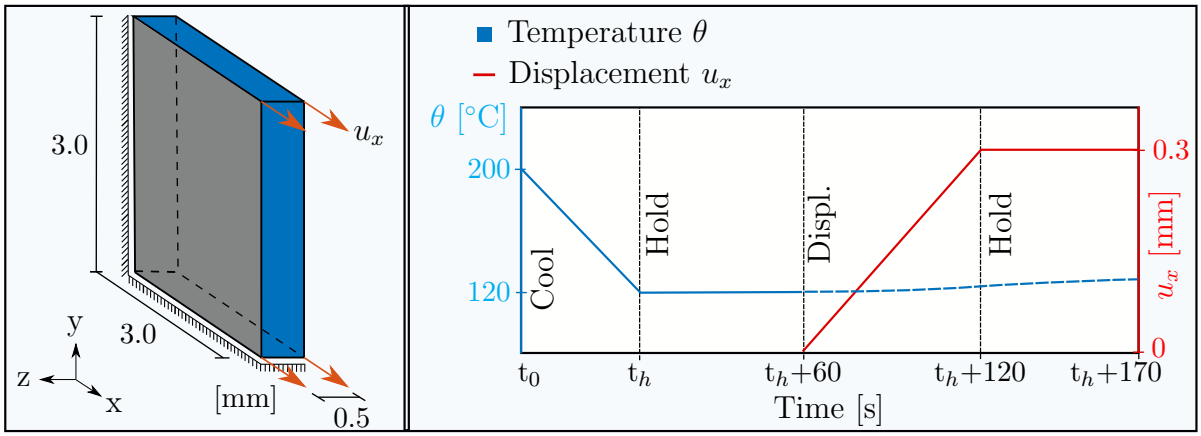

Figure 3: Geometry, boundary conditions and applied loading procedure

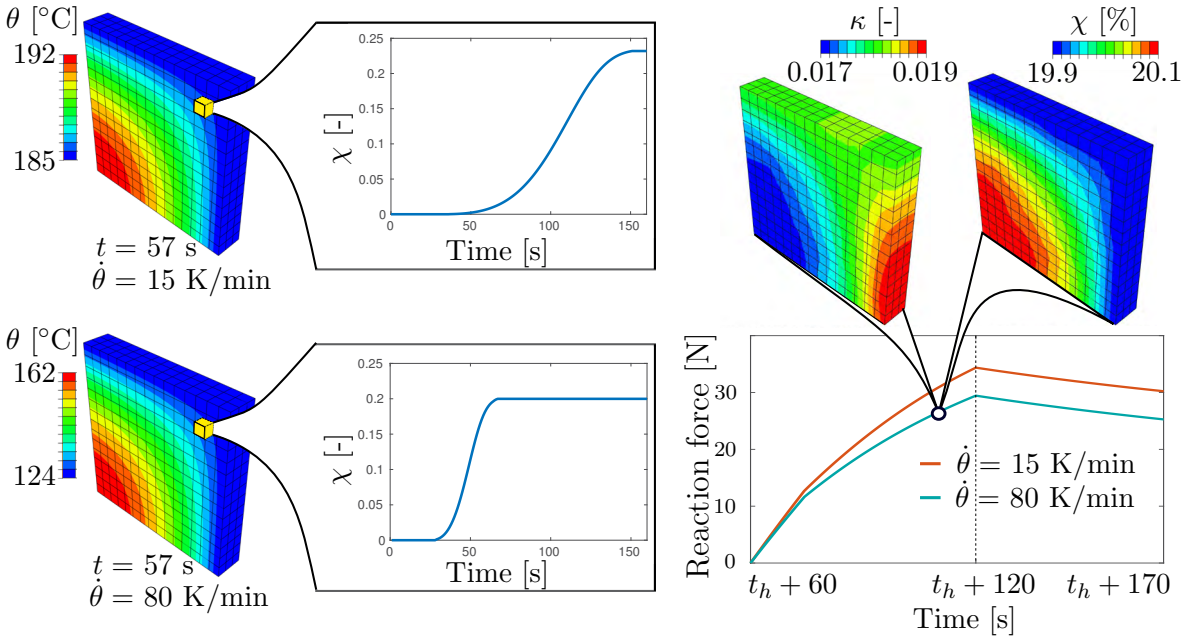

Figure 4: Reaction force, temperature θ, (evolution of) total degree of crystallinity χ and accumulated plastic strain κ

quently, a displacement is linearly increased over time until a final value of $u_x = 0.3$ mm is

prescribed. In this step, the temperature boundary conditions are removed to investigate adiabatic heating. In the last step, the displacement is held constant for 50 s to allow for relaxation. The reaction force - time relation, the total degree of crystallinity χ, the temperature θ, and the accumulated plastic strain κ for selected time steps are displayed in figure 4, for the two different loading procedures.
During the cooling phase, temperature gradients and non-constant cooling rates arise, which result in locally varying crystallisation conditions and thus in a (slightly) varying crystallinity of the structure. Consequently, the stress distribution is heterogeneous as well. Naturally, the different thermal treatments lead to a difference in the absolute degree of crystallinity for the two considered examples. The dependence of the macroscopic material behaviour on the underlying microstructure is clearly visible from the reaction force - time relation (i.e. increasing stiffness, hardening and yield stress with increasing degree of crystallinity). Furthermore, moderate adiabatic heating due to plastic and viscous dissipation is observed.

5 CONCLUSION

In the present work, a thermo-mechanically coupled and thermodynamically consistent constitutive framework at finite strains was proposed, to predict the material response of semi-crystalline polymers in the context of thermoforming processes. To account for the morphology of the underlying microstructure, the total degree of crystallinity was introduced as an additional internal variable, which contributes in an important manner to the elastic, viscous and plastic response of the material. The crystallisation kinetics during cooling from the melt are modelled by a non-isothermal modification of the Avrami model, where a static, relaxed melt is presumed. The set of material parameters is characterized for Polyamide 6 (*Ultramid B40*) and obtained from isothermal and non-isothermal DSC analysis and numerous, uniaxial tensile experiments. The experimental data and simulated behaviour is in good agreement.
The model response is demonstrated in a thermo-mechanically-coupled boundary value problem. The phenomenological approach allows to account for the complex crystallisation phenomena on the micro-scale, with sufficient accuracy. In addition, the model exhibits great convergence behaviour and numerical robustness. To the authors' knowledge, there is no comparable model available in the literature, which accounts for the thermal, mechanical and crystallisation behaviour and the corresponding complex interactions.

Acknowledgements: Financial support of the project RE 1057/41 by the German Science Foundation (DFG) is gratefully acknowledged. Furthermore, the authors are grateful for the provision of *Ultramid B40* by BASF SE.

References

[1] T.D. Fornes and D.R. Paul. Crystallization behavior of nylon 6 nanocomposites. *Polymer*, (2003) **44**:3945–3961.

[2] G. Ayoub, F. Zaïri, C. Fréderix, J.M. Gloaguen, M. Naït-Abdelaziz, R. Seguela and J.M. Lefebvre. Effects of crystal content on the mechanical behaviour of polyethylene under finite strains: Experiments and constitutive modelling. *Int. J. Plasticity*, (2011) **27**:492–511.

[3] S. Reese and S. Govindjee. A theory of finite viscoelasticity and numerical aspects. *Int. J. Solids Struct.*, (1998) **35**:3455–3482.

[4] K. Nakamura, K. Katayama and T. Amano. Some aspects of nonisothermal crystallization of polymers. II. Consideration of the isokinetic condition. *J. Appl. Polym. Sci.*,(1973) **17**:1031–1041.

[5] A. Ziabicki. *Fundamentals of Fibre Formation: The Science of Fibre Spinning and Drawing*. John Wiley & Sons Ltd, Vol. I. (1976).

[6] I. N. Vladimirov, M. P. Pietryga and S. Reese. On the modelling of non-linear kinematic hardening at finite strains with application to springback – Comparison of time integration algorithms. *Int. J. Numer. Meth. Eng.*, (2008) **75**:1–28.

[7] E. M. Arruda and M. C. Boyce. A three-dimensional constitutive model for the large stretch behavior of rubber elastic materials. *J. Mech. Phys. Solids*, (1993) **41**:389–412.

[8] W. Dettmer and S. Reese. On the theoretical and numerical modelling of Armstrong-Frederick kinematic hardening in the finite strain regime. *Comput. Method. Appl. M.*,(2004) **193**:87–116.

[9] M. Li, Y. Wan, Z. Gao, G. Xiong, X. Wang, C. Wan and H. Luo. Preparation and properties of polyamide 6 thermal conductive composites reinforced with fibers. *Mater. Design.*, (2013) **51**:257–261.

[10] B. Jurkowski, Y. A. Olkhov, K. Kelar and O. M. Olkhova. Thermomechanical study of low-density polyethylene, polyamide 6 and its blends. *Eur. Polym. J.*, (2002) **38**:1229–1236.

[11] C. Millot, L.-A. Fillot, O. Lame, P. Sotta and R. Seguela. Assessment of polyamide-6 crystallinity by DSC. *J. Therm. Anal. Calorim.*, (2015) **112**:307–314.